

TEMPERATURE MONITORING FOR LASER METAL DEPOSITION USING NEAR-INFRARED SPECTROSCOPY

Siti Qistina Arora Talib, Aneez Syuhada Mangsor, Abd Rahman Johari, Muhammad Safwan Abd Aziz, Ganesan Krishnan*

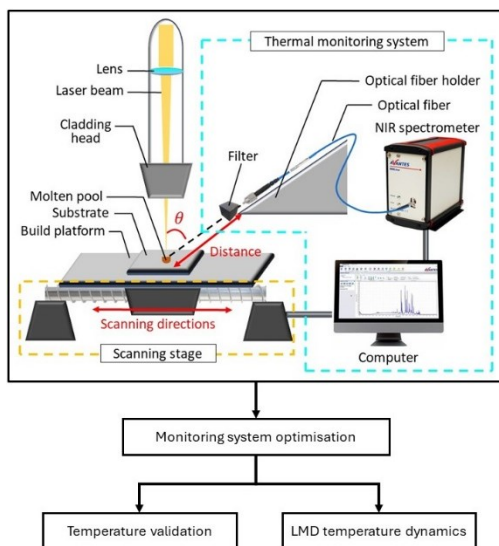
Laser Centre, Ibnu Sina Institute for Scientific and Industrial Research, Universiti Teknologi Malaysia, 81310 UTM Johor Bahru, Johor, Malaysia

Article history

Received
7 February 2024
Received in revised form
23 May 2024
Accepted
23 July 2024
Published Online
17 October 2024

*Corresponding author
k.ganesan@utm.my

Graphical abstract



Abstract

Temperature monitoring during laser metal deposition (LMD) aids process control to ensure high-quality production. However, the fluctuating emissivity of the melt pool limits the accuracy of the existing non-contact temperature measuring devices. Thus, this work explores a new temperature monitoring technique, where the thermal radiation emitted by the processing zone was collected with a near-infrared (NIR) spectrometer and fitted to Planck's law to determine the temperature. This work has established the optimised angle and distance of the fiber probe from the LMD processing area to maximise the spectral signal acquisition. The temperature determined from the technique was cross-validated with a thermocouple, resulted in a small deviation of 2.39%. The applicability of the spectroscopic method for continuous temperature monitoring of the LMD process has been demonstrated. The optimised placement for the fiber probe end was determined at the 45° angle relative to the surface of the substrate and positioned 5 cm away from the molten pool. The temperature during the LMD process decreased gradually then stabilised after approximately 17 mm track length, resembling those reports in prior studies. Our findings support the practicality of the proposed temperature monitoring approach in LMD.

Keywords: Laser Metal Deposition (LMD), temperature monitoring, thermal radiation, near-infrared (NIR) spectroscopy, Planck's Law

Abstrak

Pemantauan suhu semasa proses Laser Metal Deposition (LMD) membantu pengawalan proses bagi memastikan produksi berkualiti tinggi. Walau bagaimanapun, turun naik kepancaran takungan lebur telah menghadkan ketepatan peralatan pengukur suhu tak sentuh sedia ada. Oleh itu, projek ini menyingkap teknik pemantauan suhu baharu di mana sinaran terma yang dipancarkan oleh zon pemprosesan telah dipungut menggunakan spektrometer inframerah-dekat (NIR) dan dipadankan pada hukum Planck untuk menentukan suhu. Usaha ini menentukan sudut dan jarak unggul kuar gentian dari kawasan proses LMD bagi memaksimumkan perolehan isyarat spektrum. Suhu yang ditentukan melalui teknik ini diperiksa validasinya dengan termogandingan memutuskan bahawa terdapat sisihan kecil sebanyak 2.39%. Penerapan teknik spektroskopik ini untuk pemantauan suhu secara berterusan untuk proses LMD telah didemonstrasikan. Penempatan unggul hujung kuar gentian teroptimum adalah pada sudut 45° dari permukaan substrat dan

diletakkan 5 cm dari takungan lebur. Suhu semasa proses LMD turun secara beransur-ansur lalu stabil pada jarak runtu kira-kira 17 mm, seperti yang dilaporkan dalam kajian lain sebelum ini. Hasil kajian kami menyokong kebolehjayaan pemantauan suhu yang diusulkan semasa LMD.

Kata kunci: Laser Metal Deposition (LMD), pemantauan suhu, sinaran terma, spektroskopi inframerah-dekat (NIR), hukum Planck

© 2024 Penerbit UTM Press. All rights reserved

1.0 INTRODUCTION

In response to the growing demands for intricate geometries and expedited fabrication manufacturing components in the aerospace, medical, and automotive industries [1, 2], Additive Manufacturing (AM) techniques, particularly Laser Metal Deposition (LMD), have gained prominence. LMD originates from laser cladding (LC) [3, 4], which utilises a focused laser beam to liquefy metal powder. This process has predominantly employed cobalt alloy or bronze powders as a corrosion-resistant or wear-resistant layer [5, 6]. Furthermore, it finds application in repair scenarios, where damaged areas are machined out, and new materials such as steel or titanium are deposited as replacements [7, 8, 9]. The initial attempts made in the LC involved either a pre-placed powder bed or the use of gravity-fed powder through an external nozzle, until advancements like pneumatic powder feeders and coaxial powder nozzles bolstered the stability and efficiency of the process [10, 11, 12]. The persistent challenge in the LMD industry is the consistency of product properties. Despite employing a set of optimised processing parameters over a defined duration, suboptimal deposited material quality persists. Tang *et al.* [13] observed a pronounced "mushroom effect" in their deposited tracks, resulting in non-uniform track morphology despite consistent processing parameters during the deposition process. An escalation in substrate temperature was noted as the process advanced. Additionally, the deposition of 120 layers at a constant laser power by Bi *et al.* [14] led to wall thickness variation, attributed to fluctuations in heat conduction and heat exchange. These fluctuations significantly impacted the temperature and size of the melt pool with increasing build time.

Therefore, it is crucial to understand the thermal dynamics of LMD, which can provide insight into acquiring high-quality depositions [15, 16, 17]. The importance of precise temperature regulation in LMD processes lies in its ability to uphold process stability, thereby reducing fluctuations in material characteristics and structural imperfections [18]. This ultimately leads to achieving optimised performance parameters, encompassing mechanical properties, surface quality, and dimensional accuracy in material deposition [19, 20]. The impact of process parameters, including laser power, scan speed, and powder feeding rate, on the temperature has been extensively documented. A thorough investigation of the thermo-cycle in Laser

Powder Bed Fusion (LBF) revealed that temperature reduction occurred when the scan speed dropped below 800 mm/min due to significant evaporation from the molten pool surface [21]. Temperature exhibited a consistent upward trend with slower scanning speed and higher laser power, employed in LC and selective laser melting (SLM) [22, 23]. The elevated temperature region resembled a comet-like shape, characterized by a sharp gradient at the head of the melt pool and a lower gradient at the tail, observed where metal cooling and solidification occurred [24, 25].

However, the existing temperature monitoring techniques fall short in emphasising the crucial recognition and addressing of emissivity sensitivity to surface characteristics during the monitoring process. Thermal cameras, valued for providing detailed spatial temperature distribution in the deposition region, faced a challenge to determine accurate temperature during LMD process due to variation of emissivity. This emissivity variation becomes severe at high temperatures because of the frequent occurrence of cracks in the deposited layer [26, 27]. Meanwhile, pyrometers offer versatility for non-contact temperature measurement, a crucial feature for dynamic additive manufacturing technology. A study employing two pyrometers at 1kHz frequency to measure the molten pool's temperature reported consistent readings under various input parameters [28]. However, Galkin *et al.* [29] pointed out that challenges arose in establishing a precise relationship between pyrometry readings and actual temperatures due to the high-speed nature of the measurement and variations in emissivity. Conversely, thermocouples, acting as contact-based temperature measuring devices, were successfully demonstrated in a LMD system. An approach entailed the insertion of K-type thermocouples into machined holes at various depths within the material [30]. Although K-type thermocouples offer a high precision of $\pm 2.2^{\circ}\text{C}$, it is essential to recognize a significant limitation: the thermal conductivity mechanism of thermocouples may cause delays in precisely measuring material temperatures, potentially impacting the timeliness and precision of temperature readings in scenarios with swift temperature variations. While effective in predicting material characteristics, this method demands a complex setup.

In response to this gap, this study introduces an approach using near-infrared (NIR) spectroscopy captured thermal radiation spectrum, processed to a refined spectrum, which then produced Planck's

radiation fit to determine the LMD process temperatures. This is due to its capability to overcome the challenge of fluctuating emissivity and offer a non-contact measurement, which is independent of the thermal conductivity mechanism that can lead to delays in accurately measuring material temperatures in situations with rapid temperature changes. The implementation of a near-infrared spectroscopy system for temperature measurement during LMD through Planck's law fitting to the acquired thermal radiation spectrum can enhance temperature measurement accuracy and consistency. This method offers a non-contact temperature measuring technique independent of the emissivity of the LMD molten pool.

2.0 METHODOLOGY

2.1 Laser Metal Deposition System

The laser metal deposition system consists of a laser beam source (RFL-C1500, Wuhan Raycus Fiber Laser Technologies Co., Ltd.) of 1.5 kW continuous-wave ytterbium fiber laser, operating at a wavelength of 1080 ± 5 nm. The complete LMD system used is shown in Figure 1. A focused laser beam energy was required as a heating source to melt the Ti-6Al-4V feedstock powder (Sichuan Porous Metal Technology Co., Ltd.) with a particle size range of $15 \mu\text{m}$ to $53 \mu\text{m}$ flowing from the coaxial powder-fed system. Subsequently, the heating formed a molten pool on the Ti-6Al-4V substrate plate with dimensions of $3 \text{ mm} \times 20 \text{ mm} \times 30 \text{ mm}$ (height \times width \times length). Argon gas was utilised as shielding and carrier gas to deposit the single layer track to the laser processing area. The substrate was placed on a scanning stage to provide motion control over the build platform with a scanning speed range of 100 mm/min to 2000 mm/min. The scanning stage allowed precise control of the laser beam's path and the deposition pattern on the build surface.

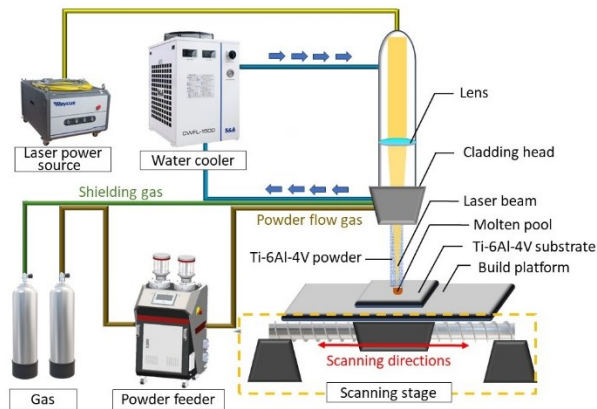


Figure 1 Schematic diagram of LMD system

2.2 Responsivity Measurement

The thermal radiation spectrum was gathered by a near-infrared (NIR) spectroscopy system that consists of

a fibre probe, filter and NIR spectrometer. It is crucial to obtain the responsivity at each wavelength of the spectroscopy system using a reference spectral source [31, 32]. Thus, a stabilised tungsten halogen light source (Thorlabs SLS201/M) output spectrum was collected using a bandpass filter fitted optical fiber probe (600 μm -SMA905 Energy Fiber, XINRUI) that was connected to a NIR spectrometer (NIR256-1.7-EVO, Avantes) as depicted in Figure 2.

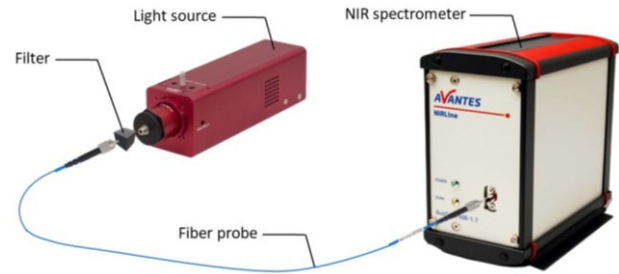


Figure 2 Responsivity measurement setup

The filter with transmission window, approximately from 1300 nm to 1600 nm, was placed at one of the ends of the optical fiber to block the laser output of 1080 nm from entering the spectrometer. The spectral absorption contributed by the filter must be removed to reveal the profile of infrared radiation of the molten pool. Thus, including the filter in the responsivity measurement setup was significant.

2.3 Fiber Probe Placement Optimisation

The optical fiber used to capture the thermal radiation spectrum of the molten pool was susceptible to damage by the laser spatters during the LMD process. It was vital to place the probe securely at an optimal position while minimising the risk of probe fiber damage with the imperative of maximising data collection efficiency. Hence, experimental works were conducted to determine the optimised position of the probe by varying the fiber probe angle with respect to the laser beam and the distance between the fiber probe end and the molten pool, as shown in Figure 3. Initially, the fiber probe angle was varied from 45° to 90° to determine the angle at which the maximum thermal radiation signal was collected. Subsequently, by placing the probe at the optimal probe angle, the probe distance was varied from 5 cm to 9 cm to determine the optimal probe distance.

The LMD processes were done with the scanning speed, laser power, powder feedstock flow, and shielding gas flow of 100 mm/s, 450 W, 10 g/min, and 5 Pa, respectively. Once the LMD process was operated, the spectral reading at each fiber placement was taken at 1 cm deposition track length with the averaging and integration time of the spectrometer set to 1 and 0.02 ms, respectively.

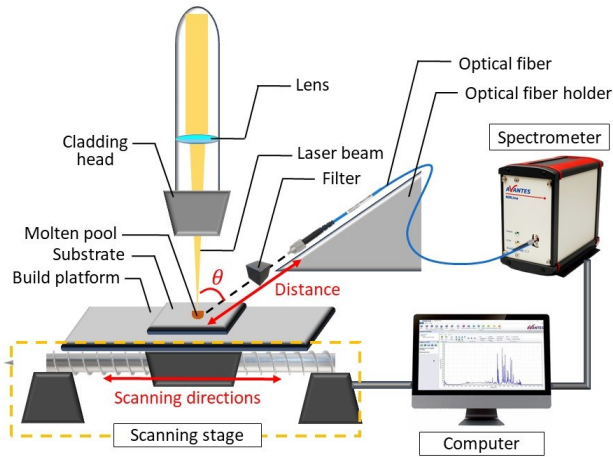


Figure 3 LMD setup for probe positioning optimisation

2.4 Temperature Determination from NIR Spectral Data

The raw NIR spectral data $I_{raw}(\lambda_n)$ collected must be calibrated by factoring in the responsivity $R(\lambda_n)$ for each wavelength. The responsivity was determined using Equation 1,

$$R(\lambda_n) = \frac{S_{obt}(\lambda_n)}{S_{ref}(\lambda_n)} \quad (1)$$

where $S_{obt}(\lambda_n)$ is the collected spectral data of the reference SLS201/M light source and $S_{ref}(\lambda_n)$ is the known spectrum of the light source provided by the manufacturer. The raw intensity, $I_{raw}(\lambda_n)$, of the collected thermal radiation must be calibrated by factoring in the responsivity according to Equation 2 before the temperature determination process.

$$I_{cal}(\lambda_n) = \frac{I_{obt}(\lambda_n)}{R(\lambda_n)} \quad (2)$$

The temperature T for the processing area was determined from the spectral data collected using Planck's radiation law as expressed in Equation 3,

$$I_{cal}(\lambda_n) = \varepsilon \frac{2hc^2}{\lambda_n^5} \times \left[\exp\left(\frac{hc}{\lambda_n kT}\right) - 1 \right]^{-1} \quad (3)$$

where h is Planck's constant, ε is the emissivity and k is the Boltzmann constant. The Gnuplot software was used to fit Planck's radiation law to the thermal radiation spectrum collected, where the temperature T and emissivity ε were set as the fitting parameters.

2.5 Temperature Validation for NIR Spectroscopic Method

A setup was devised to compare the temperature readings of a heated constantan wire determined via a thermocouple and the NIR spectroscopy temperature determination method in this work. This comparative approach aimed to assess the accuracy and reliability of the temperature reading obtained

from the thermal radiation spectrum by juxtaposing them with the temperature determined by the thermocouple. As illustrated in Figure 4, the experimental setup involved connecting the N-type thermocouple to a multimeter. The constantan wire connected to a 3 V DC power supply was coiled at the sensing end of the thermocouple. With a current supply of 6 A, the constantan wire was heated to appear bright red. As the multimeter displayed a consistent voltage reading, signifying that the wire had reached equilibrium temperature, a single spectrum was captured by the spectrometer, and the multimeter reading was recorded simultaneously. The temperature from the thermocouple was deduced by referencing the measured voltage output to the thermocouple N-type voltage-temperature table provided by the manufacturer.

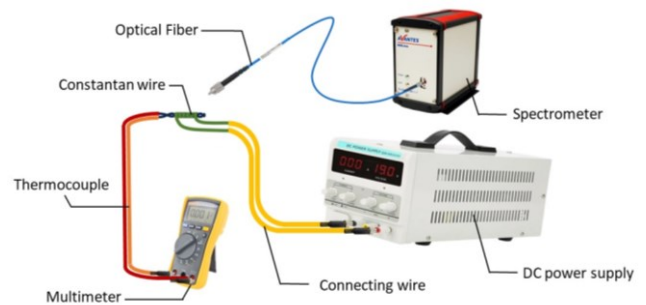


Figure 4 Temperature determination of a heated constantan wire setup

2.6 Temperature Variation Determination during LMD Process

Upon determining the optimised placement of the fiber probe through the angle and distance optimisation process as outlined in Section 2.3, the finalised configuration was implemented in the continuous temperature monitoring of the LMD process. The LMD process was conducted with consistent input parameters, similarly in Section 2.3. Spectra were continuously acquired before initiating the LMD operation, with an averaging time set to one and an integration time set to 0.02 ms. A deposition track of 20 mm was created during the LMD process. The laser was deactivated upon reaching a track length of 20 mm, at which point the acquisition of spectra was also halted. Subsequently, data processing to determine the deposition temperature at each instant was executed following the procedures outlined in Section 2.4, providing insights into the temperature variation during the LMD process.

3.0 RESULTS AND DISCUSSION

Figure 5 displays the thermal radiation spectrum across various probe angles where each probe angle exhibited the same spectral pattern. However, the

intensities of the spectrum escalated at smaller probe angles. The rise observed in the graph indicates that the field of view (FOV) of the probe residing on the deposited area at a smaller angle, as opposed to a bigger angle where the focus shifts towards the airborne melting powder during the LMD process. The deposited area mentioned includes both the molten pool and the surface of the deposited track.

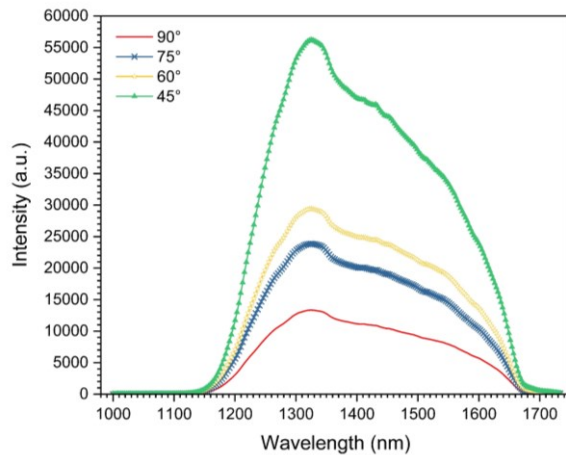


Figure 5 Raw thermal radiation spectra at varying probe angles

For instance, at a 90° angle, the molten pool is not visible to the probe, leading to most of the intensity received from the airborne melting powder. On the other hand, at a 45° angle, the top view of the deposited area becomes apparent to the probe, shifting its FOV to the deposited area instead. Thus, this angle captures more thermal radiation from the deposited area compared to a 90° angle. This resulted in the 45° angle as the optimal choice for the probe angle to capture the highest intensity of thermal radiation emitted from the deposited area.

Figure 6 exhibits the thermal radiation spectra for various probe distances. The intensity decreased as the probe distance increased from 5 cm to 9 cm. The inset of Figure 6 displays the intensity for the wavelength of 1318.863 nm, showing a prominent decreasing pattern as the distance increased. The intensity experimental data ranging from 6 cm to 9 cm fitted with the inverse square law at $162.833/r^2$ where r is the distance away from the centre of the processing area. Within this distance range, the FOV of the fiber probe captures the thermal radiation emitting from both, the deposited region and the substrate. Meanwhile, the 5 cm data deviated from the theoretical trend because of its smaller FOV, focusing on the deposited region only. Despite this deviation, the intensity captured at a 5 cm probe distance registers as the highest. Consequently, the optimal probe placement distance was determined to be 5 cm for capturing the maximum intensity.

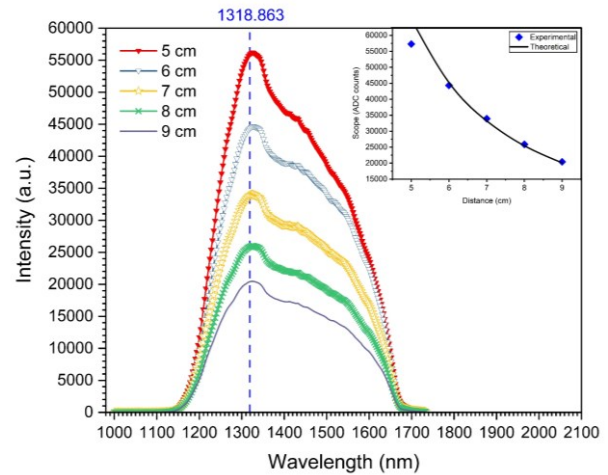


Figure 6 Raw thermal spectra captured with varying distances at a 45° angle, and (inset figure: intensity at 1318.863 nm for each distance graph)

The raw thermal radiation spectrum of a stabilised tungsten halogen light source is shown in Figure 7, alongside its reference spectrum from the manufacturer and the responsivity curve of the NIR spectroscopic system. Despite the reference spectrum steadily declining pattern, the raw spectral of the light source captured by the fiber probe showed a curve with a peak at 1318.863 nm instead. Thus, due to the prominent pattern difference between the two spectral curves, the responsivity of each wavelength of the thermal radiation spectrum captured was factored in, as in Equation 2. This was done to reveal the calibrated thermal radiation spectrum emitted from the processing zone.

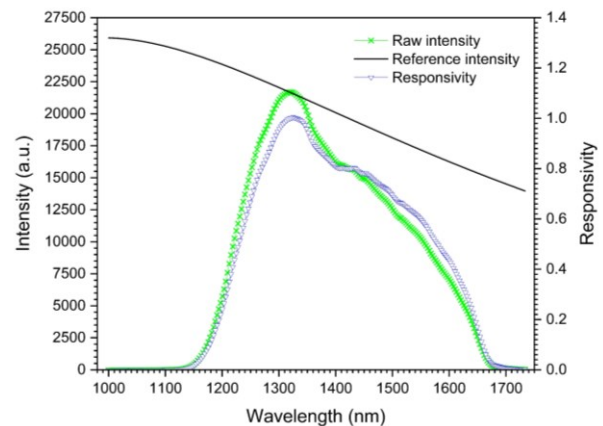


Figure 7 The light source reference spectrum, raw thermal spectrum captured, and the responsivity curve of the NIR spectroscopic system

In contrast to the reference spectrum, the responsivity curve mirrored the pattern observed in the raw thermal radiation spectrum, featuring a prominent peak at 1324.847 nm. Notably, the responsivity curve registered close to null values between 1650 nm and 1750 nm,

denoting that the detector is unresponsive to these wavelengths. A similar pattern was perceived in the wavelength of 1000 to 1150 nm, but primarily due to the high filter absorbance in that region. As a result, subsequent spectral analysis in the temperature determination study only included the wavelengths from 1300 nm to 1650 nm. This range corresponded to the filter transmission window, ensuring responsive data for further analysis.

The raw spectrum captured deposition using the optimal probe placement at the distance of 5 cm and angle of 45° was processed to demonstrate the NIR spectroscopy temperature determination method. Figure 8 depicts three spectra: raw spectrum captured, calibrated spectrum after factoring in the responsivity value, and a fit with Planck's radiation law. The calibrated spectrum fitted at 2028.14 ± 6.639 K.

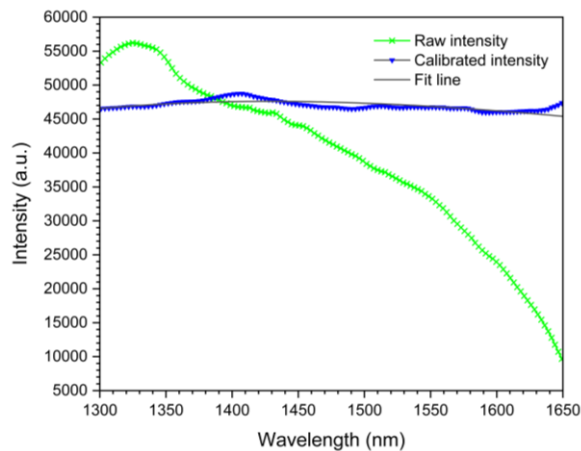


Figure 8 Temperature determination from thermal radiation captured 5 cm away at a 45° angle relative to the laser beam

To validate this spectroscopy temperature determination method, the method was compared to the thermocouple method. Figure 9 displays the results of the captured thermal radiation spectrum emitted by a uniformly heated constantan wire were processed. The raw spectrum captured was refined and generated a Planck's radiation with the temperature at 1228.02 ± 3.273 K. Meanwhile, the N-type thermocouple, provided a reference temperature, evoked an output voltage of 25.3 mV, which was equivalent to 1199.43 K. The relatively small percentage difference of approximately 2.36% between the two temperatures highlights the reliability of the NIR spectroscopy temperature determination method.

Figure 10 presents the temperature profile over the deposited track distance throughout the LMD process with optimal fiber probe placement. At a track distance of 0.83 mm, the sudden rise in temperature signifies the initiation of the laser during the process. This temperature spike is primarily influenced by the thermal radiation emitted by the deposited surface. As the process progresses, heat begins to disperse across the substrate and the deposited layer. Consequently, the temperature was observed to decline gradually,

reaching an equilibrium of around 1900 K. The overall thermal dynamics pattern agrees with the results reported by de La Batut *et al.* [33].

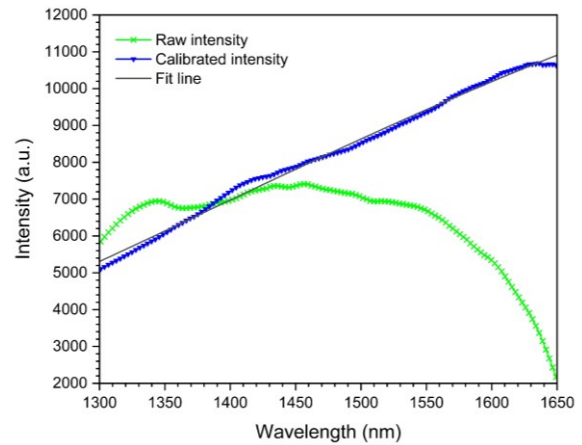


Figure 9 Captured thermal radiation spectrum of a heated constantan wire processed to a refined spectrum, producing Planck's radiation fit

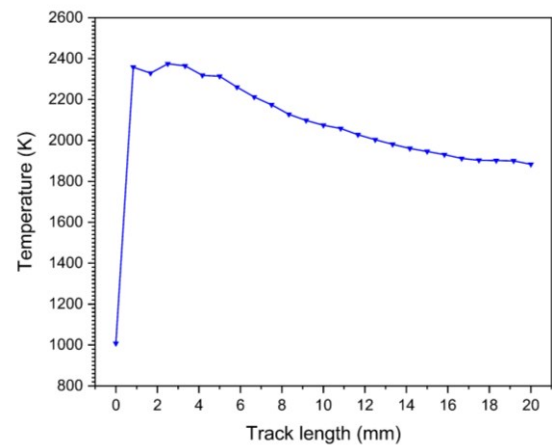


Figure 10 Temperature variation across the deposited track during the LMD process

4.0 CONCLUSION

The demonstrated near-infrared spectroscopy temperature monitoring system showcased optimal functionality when the fiber probe was placed at a 45° angle relative to the substrate surface and positioned 5 cm away from the molten pool. By comparing this spectroscopic approach for temperature determination with thermocouples, the presented method was able to provide a highly correlated temperature value within a verification precision of 2.39%. The thermal dynamics recorded with the presented approach had a similar pattern as reported in previous research. Therefore, our study has sufficiently demonstrated the efficacy of the NIR spectroscopy temperature determination method for a LMD system. The results presented in this work mainly focused on the feasibility of spectroscopic methods in temperature

determination during LMD process and the result revealed the high potential of this method due to its accuracy and ease of implementation in existing LMD systems. However, more studies need to be done to improve the accuracy further and to expand its versatility. In future works, one may include the temperature variation across the molten pool to improve the fitting model and determine highly accurate temperatures. Also, it is possible to determine the variation of emissivity of the deposited layer from the spectrum recorded to give real-time feedback on the surface quality of the deposited layer.

Acknowledgement

This research was supported by the Ministry of Education Malaysia and Universiti Teknologi Malaysia through UTM RA Iconic Grant, cost center no. Q.J130000.4354.09G60 and UTM Encouragement Research, cost center no. Q.J130000.3854.31J74. The first author also wishes to thank the Ministry of Education Malaysia for providing MyBrainSc Scholarship for her postgraduate study.

Conflicts of Interest

The author(s) declare(s) that there is no conflict of interest regarding the publication of this paper.

References

- Wanjara, P., Backman, D., Sikan, F., Gholipour, J., Amos, R., Patnaik, P., et al. 2022. Microstructure and Mechanical Properties of Ti-6Al-4V Additively Manufactured by Electron Beam Melting with 3D Part Nesting and Powder Reuse Influences. *Journal of Manufacturing and Materials Processing*. 16(1): 21. Doi: <https://doi.org/10.3390/jmmp6010021>.
- Zhang, L. C., Chen, L. Y., Zhou, S., Luo, Z. 2023. Powder Bed Fusion Manufacturing of Beta-type Titanium Alloys for Biomedical Implant Applications: A Review. *J Alloys Compd*. 936: 168099. Doi: <https://doi.org/10.1016/j.jallcom.2022.168099>.
- Diegel, O., Nordin, A., Motte, D. 2019. *A Practical Guide to Design for Additive Manufacturing*. Singapore: Springer Singapore. Doi: <https://doi.org/10.1007/978-981-13-8281-9>.
- Frazier, W. E. 2014. Metal Additive Manufacturing: A Review. *J Mater Eng Perform*. 8: 23(6): 1917-28. Doi: <https://doi.org/10.1007/s11665-014-0958-z>.
- Koshy, P. 1985. Laser Cladding Techniques for Application to Wear and Corrosion Resistant Coatings. In: Jacobs, R. R., (Ed.). 80. Doi: <https://doi.org/10.1117/12.946398>.
- Smoqi, Z., Toddy, J., Halliday, H. (Scott), Shield, J. E., Rao, P. 2021. Process-structure Relationship in the Directed Energy Deposition of Cobalt-chromium Alloy (Stellite 21) coatings. *Mater Des*. 197: 109229. Doi: <https://doi.org/10.1016/j.matdes.2020.109229>.
- Brandt, M., Sun, S., Alam, N., Bendeich, P., Bishop, A. 2009. Laser Cladding Repair of Turbine Blades in Power Plants: From Research to Commercialisation. *International Heat Treatment and Surface Engineering*. 13(3): 105-14. Doi: <https://doi.org/10.1179/174951409X12542264513843>.
- Graf, B., Gumenyuk, A., Rethmeier, M. 2012. Laser Metal Deposition as Repair Technology for Stainless Steel and Titanium Alloys. *Phys Procedia*. 39: 376-81. Doi: <https://doi.org/10.1016/j.phpro.2012.10.051>.
- Torims, T. 2013. The Application of Laser Cladding to Mechanical Component Repair. *Renovation and Regeneration*. 587-608. Doi: <https://doi.org/10.2507/daaam.scibook.2013.32>.
- Gnanamuthu, D. 1980. S. Laser Surface Treatment. *Optical Engineering*. 19(5): 783-92. Doi: <https://doi.org/10.1117/12.7972604>.
- Eboo, G. M., Lindemanis, A. E. 1985. Advances in Laser Cladding Process Technology. In: Applications of High Power Lasers. *SPIE*. 86-94. Doi: <https://doi.org/10.1117/12.946399>.
- Vetter, P. A., Fontaine, J., Engel, T., Lagrange, L., Marchione, T. 1970. Characterization of Laser-material Interaction during Laser Cladding Process. *WIT Transactions on Engineering Sciences*. 2.
- Tang, L., Landers, R. G. 2010. Melt Pool Temperature Control for Laser Metal Deposition Processes-Part I: Online Temperature Control. *J. Manuf. Sci. Eng*. 132(1): 011010 Doi: <https://doi.org/10.1115/1.4000882>.
- Bi, G., Gasser, A., Wissenbach, K., Drenker, A., Poprawe, R. 2006. Characterization of the Process Control for the Direct Laser Metallic Powder Deposition. *Surf Coat Technol*. 201(6): 2676-83. Doi: <https://doi.org/10.1016/j.surfcoat.2006.05.006>.
- Yamashita, Y., IIman, K. A., Kunimine, T., Sato, Y. 2023. Temperature Evaluation of Cladding Beads and the Surrounding Area during the Laser Metal Deposition Process. *Journal of Manufacturing and Materials Processing*. 7(6): 192. Doi: <https://doi.org/10.3390/jmmp7060192>.
- Mazzarisi, M., Campanelli, S. L., Angelastro, A., Palano, F., Dassisti, M. 2021. In situ Monitoring of Direct Laser Metal Deposition of a Nickel-based Superalloy using Infrared Thermography. *The International Journal of Advanced Manufacturing Technology*. 112: 157-73. Doi: <https://doi.org/10.1007/s00170-020-06344-0>.
- Yan, Z., Liu, W., Tang, Z., Liu, X., Zhang, N., Li, M., et al. 2018. Review on Thermal Analysis in Laser-based Additive Manufacturing. *Opt Laser Technology*. 106: 427-41. Doi: <https://doi.org/10.1016/j.optlastec.2018.04.034>.
- L. Qin, K. Wang, X. Li, S. Zhou, and G. Yang. 2022. Review of the Formation Mechanisms and Control Methods of Geometrical Defects in Laser Deposition Manufacturing. *Chinese Journal of Mechanical Engineering: Additive Manufacturing Frontiers*. 1(4): 100052. Doi: <https://doi.org/10.1016/j.cjmeam.2022.100052Y>.
- Y. N. Kulchin et al. 2022. Melt Pool Temperature Control in Laser Additive Process. *Bulletin of the Russian Academy of Sciences: Physics*. 86(Suppl 1): S108-S113. Doi: <https://doi.org/10.3103/S1062873822700496>.
- C. Zheng, J. T. Wen, and M. Diagne. 2020. Distributed Temperature Control in Laser-based Manufacturing. *J Dyn Syst Meas Control*. 142(6). Doi: 10.1115/1.4046154.
- Muvvala, G., Karmakar, D. P., Nath, A. K. 2017. Online Monitoring of Thermo-cycles and Its Correlation with Microstructure in Laser Cladding of Nickel Based Super Alloy. *Opt Lasers Eng*. 88: 139-52. Doi: <https://doi.org/10.1016/j.optlaseng.2016.08.005>.
- Ju, H., Xu, P., Lin, C., Sun, D. 2015. Test and Temperature Field of Finite Element Simulation about the Effect of Scanning Speed on 304 Stainless Layer's Properties by Laser Cladding. *Materials Research Innovations*. 19(sup8): S8-9. Doi: <https://doi.org/10.1179/1432891715Z.0000000001605>.
- Manvatkar, V., De A, DebRoy, T. 2015. Spatial Variation of Melt Pool Geometry, Peak Temperature and Solidification Parameters during Laser Assisted Additive Manufacturing Process. *Materials Science and Technology*. 31(8): 924-30. Doi: <https://doi.org/10.1179/1743284714Y.00000000701>.
- Gu, D., Yuan, P. 2015. Thermal Evolution Behavior And Fluid Dynamics during Laser Additive Manufacturing of Al-based

- Nanocomposites: Underlying Role of Reinforcement Weight Fraction. *J Appl Phys.* 118(23).
Doi: <https://doi.org/10.1063/1.4937905>.
- [25] Doubenskaia, M., Pavlov, M., Grigoriev, S., Smurov, I. 2013. Definition of Brightness Temperature and Restoration of True Temperature in Laser Cladding using Infrared Camera. *Surf Coat Technol.* 220: 244-7.
Doi: <https://doi.org/10.1016/j.surfcoat.2012.10.044>.
- [26] Mazzarisi, M., Angelastro, A., Latte, M., Colucci, T., Palano, F., Campanelli, S. L. 2023. Thermal Monitoring of Laser Metal Deposition Strategies using Infrared Thermography. *J Manuf Process.* 85: 594-611.
Doi: <https://doi.org/10.1016/j.jmapro.2022.11.067>.
- [27] Altenburg, S. J., Straße, A., Gumenyuk, A., Maierhofer, C. 2022. In-situ Monitoring of a Laser Metal Deposition (LMD) Process: Comparison of MWIR, SWIR and High-speed NIR Thermography. *Quant Infrared Thermogr J.* 19(2): 97-114.
Doi: <https://doi.org/10.1080/17686733.2020.1829889>.
- [28] Nair, A. M., Muvvala, G., Sarkar, S., Nath, A. K. 2020. Real-time Detection of Cooling Rate using Pyrometers in Tandem in Laser Material Processing and Directed Energy Deposition. *Mater Lett.* 277: 128330.
Doi: <https://doi.org/10.1016/j.matlet.2020.128330>.
- [29] Galkin, G., Gawade, V., Guo, W., Yi, J., Guo, Y. B. 2022. In-Situ and Real-Time 3D Pyrometry for Thermal History Diagnosis in Laser Fusion Process. *Manuf Lett.* 33: 862-71.
Doi: <https://doi.org/10.1016/j.mfglet.2022.07.106>.
- [30] Ya, W. 2015. Laser Materials Interactions during Cladding: Analyses on Clad Formation, Thermal Cycles, Residual Stress and Defects. PhD Thesis. Faculty of Engineering Technology.
- [31] Koruba, P., Ćwikła, M., Zakrzewski, A., Jurewicz, P., Reiner, J. Spectral analysis of thermal emission from melt pool during laser material processing. Technical Paper and Presentations. Wrocław University of Science and Technology, Wrocław, Poland.
- [32] De Baere, D., Devesse, W., De Pauw, B., Smeesters, L., Thienpont, H., Guillaume, P. 2016. Spectroscopic Monitoring and Melt Pool Temperature Estimation during the Laser Metal Deposition Process. *J Laser Appl.* 28(2).
Doi: <https://doi.org/10.2351/1.4943995>.
- [33] De La Batut, B., Fergani, O., Brotan, V., Bambach, M., El Mansouri, M. 2017. Analytical and Numerical Temperature Prediction in Direct Metal Deposition of Ti6Al4V. *Journal of Manufacturing and Materials Processing.* 1(1): 3.
Doi: <https://doi.org/10.3390/jmmp1010003>.